Water Research X 12 (2021) 100106

Contents lists available at ScienceDirect

Water Research X

journal homepage: www.sciencedirect.com/journal/water-research-x

Engineered methanotrophic syntrophy in photogranule communities removes dissolved methane

Anissa Sukma Safitri [a], Jérôme Hamelin [b], Roald Kommedal [a], Kim Milferstedt [b,*]

[a] Department of Chemistry, Bioscience and Environmental Engineering, University of Stavanger, 4036 Stavanger, Norway
[b] INRAE, Univ Montpellier, LBE, 102 Avenue des Etangs, 11100, Narbonne, France

ARTICLE INFO

Keywords:
Dissolved methane
interactions
bioaugmentation
ecological engineering
effluent polishing
anaerobic digestion

ABSTRACT

The anaerobic treatment of wastewater leads to the loss of dissolved methane in the effluent of the treatment plant, especially when operated at low temperatures. The emission of this greenhouse gas may reduce or even offset the environmental gain from energy recovery through anaerobic treatment. We demonstrate here the removal and elimination of these comparably small methane concentrations using an ecologically engineered methanotrophic community harbored in oxygenic photogranules. We constructed a syntrophy between methanotrophs enriched from activated sludge and cyanobacteria residing in photogranules and maintained it over a two-month period in a continuously operated reactor. The novel community removed dissolved methane during stable reactor operation by on average 84.8±7.4% (±standard deviation) with an average effluent concentration of dissolved methane of 4.9±3.7 mg $CH_4 \cdot l^{-1}$. The average methane removal rate was 26 mg $CH_4 \cdot l^{-1} \cdot d^{-1}$, with an observed combined biomass yield of 2.4 g VSS·g CH_4^{-1}. The overall COD balance closed at around 91%. Small photogranules removed methane more efficiently than larger photogranule, likely because of a more favorable surface to volume ratio of the biomass. MiSeq amplicon sequencing of 16S and 23S rRNA revealed a potential syntrophic chain between methanotrophs, non-methanotrophic methylotrophs and filamentous cyanobacteria. The community composition between individual photogranules varied considerably, suggesting cross-feeding between photogranules of different community composition. Methanotrophic photogranules may be a viable option for dissolved methane removal as anaerobic effluent post-treatment.

Introduction

The use of anaerobic granulated biomass for biological wastewater treatment was introduced about 40 years ago (Lettinga et al., 1980), and is now regarded an adequate methodology for municipal wastewater treatment (Seghezzo et al., 1998) and energy recovery (Gao et al., 2014). The development of anaerobic wastewater treatment since the end of the 1990s has been considered a more sustainable alternative to traditional aerobic processes, especially for high strength wastewater. Its primary purpose is the conversion of organic matter to methane as a renewable form of energy (Vandevivere, 1999; Verstraete et al., 1996).

An often-overlooked drawback of anaerobic wastewater treatment is the loss of dissolved methane as not all of it partitions to the gas phase inside the digesters. Estimations of the loss of dissolved methane from anaerobic wastewater treatment are typically calculated from methane concentrations in the gaseous headspace using Henry's Law, i.e., under equilibrium conditions (Lobato et al., 2012). This idealized case does not always reflect the actual measured values of anaerobic treatment liquid effluent as mass-transfer limitations can lead to supersaturation of methane. In this case, an assumed equilibrium with headspace concentrations will thus underestimate the dissolved methane content. Souza et al. (2011) and Wu et al. (2017) found that dissolved methane was supersaturated in the liquid phase of an anaerobic bioreactor effluent (saturation factor of 1.03–1.67), increasing with the increased methane solubility at decreasing temperatures. Even at equilibrium, considerable amounts of methane are lost with the liquid effluent, especially when treating wastewater at low temperatures and/or in high-flow through situations (low hydraulic retention time) (Brandt et al., 2019). Once the effluent is discharged and exposed to ambient methane partial pressures, methane degasses into the atmosphere.

Theoretically, 0.38 liters of methane are produced per gram of chemical oxygen demand (COD) removed from the anaerobic wastewater treatment at standard ambient condition (25°C, 1 atm) (Tchobanoglous et al., 2003). By assuming 80% COD removal efficiency for a

* Corresponding author
E-mail address: kim.milferstedt@inrae.fr (K. Milferstedt).

https://doi.org/10.1016/j.wroa.2021.100106
Received 1 January 2021; Received in revised form 3 June 2021; Accepted 5 June 2021
Available online 9 June 2021

typical high strength municipal wastewaters with an average soluble COD concentration of 450 $g \cdot m^{-3}$ (Henze et al., 2008), 137 l $CH_4 \cdot m^{-3}$ is produced, equivalent to 89.7 g $CH_4 \cdot m^{-3}$. At a methane solubility of approximately 20 $g \cdot m^{-3}$ at 25°C (Liu et al., 2014), approximately 22% of all produced methane would be in its dissolved form and likely leave the digester. At most about 107 l $CH_4 \cdot m^{-3}$ could be used for combustion, saving fossil CO_2 emissions of 107 l $CO_2 \cdot m^{-3}$. Degassing of the dissolved methane to the atmosphere, however, would contribute approximately 500 g $CO_{2\ equiv} \cdot m^{-3}$, equivalent to 278 l $CO_2 \cdot m^{-3}$. Therefore, the greenhouse gas contribution in this example is about 2.5 times greater than the positive effects from generating a renewable energy (see Supplemental Materials). This methane loss is significantly reducing and, as in the given example, even offsetting the positive effect of energy recovery from anaerobic wastewater treatment. Therefore, a post-treatment process is required to remove dissolved methane, reducing the environmental impact of anaerobic wastewater treatment. Several methods have been proposed for removing or recovering dissolved methane from anaerobic effluents. These include air stripping oxidation (Hatamoto et al., 2010; Matsuura et al., 2015) and degassing membrane-based recovery (Bandara et al., 2011; Cookney et al., 2016).

Dissolved methane can be biologically oxidized by methanotrophs. Methanotrophs are part of a larger group of bacteria called methylotrophs that typically utilize single-carbon compounds like methane, methanol, formic acid or even formaldehyde as carbon and energy source (Chistoserdova et al., 2009). Methanotrophs may fully oxidize methane to CO_2 or partially to molecules like methanol. Molecular oxygen is required for the conversion. Through the coupled activities of eukaryotic algae or photosynthetic bacteria and methanotrophs in syntrophic bioaggregates, oxygen may be provided by direct, or at least local transfer. The produced oxygen is then immediately utilized by the methanotrophs to convert organic matter to CO_2 which is in turn used by phototrophs for autotrophic CO_2 fixation. These interactions are found in natural systems, for example, at the chemocline between anaerobic and aerobic water layers in freshwater lakes (Milucka et al., 2015), and are also utilized in engineered systems, e.g., by van der Ha et al. (2012) for the production of lipids or polyhydroxy butyrate using co-cultured eukaryotic algae and methanotrophs. Rasoulie et al. (2018) also investigated a co-culture of green microalgae and methanotrophs for removing methane and recovering nutrients. They used industrial wastewater as media and synthetic biogas as methane source. In both studies, the authors used pure cultures of methanotrophs and microalgae (Rasouli et al., 2018; van der Ha et al., 2012). In nature, methanotrophs often co-occur with non-methanotrophic methylotrophs that feed on partially oxidized methane intermediates like methanol (Takeuchi et al., 2019; Yu et al., 2017). These more complex interactions are also relevant in our study using an environmental enrichment as basis for the construction of a new syntrophy.

In contrast to studies using suspended phototrophic-methanotrophic consortia, we present here an aggregated biomass in the form of photogranules for the aeration-free removal of dissolved methane. The conversion relies on syntrophic interactions between phototrophic cyanobacteria and methanotrophic bacteria aggregated in oxygenic photogranules. Aggregation is particularly important in the bioprocesses as it allows efficient and fast removal of the biomass from the treated water and efficient intra-aggregate oxygen transfer. We established the presence of methanotrophic bacteria in the photogranule aggregates and propagated the newly developed syntrophy in an open community, challenged by invading microbes. The syntrophy was ecologically engineered from an enrichment culture of methanotrophs from activated sludge and oxygenic photogranules converting synthetic wastewater, as described in Milferstedt et al. (2017). We discuss community assembly in the light of performance characteristics of a continuously operated reactor system for the removal of dissolved methane.

Materials and Methods

Media composition

The media composition for the batch experiments (i.e., enrichment and size specific analysis) and for the continuously operated reactor were identical, a modified nitrate mineral salt (NMS) solution (Whittenbury et al., 1970). The nutrient content of the NMS media was modified by increasing the phosphate concentration and replacing nitrate with ammonium as nitrogen sources to mimic effluents from anaerobic processes. The media was prepared and diluted with tap water which naturally containing approximately 4 mM as bicarbonate (HCO_3^-). The final concentrations in the feed were as following: 150 $mg \cdot l^{-1}$ of NH_4Cl, 20 $mg \cdot l^{-1}$ of $MgSO_4 \cdot 7H_2O$, 4 $mg \cdot l^{-1}$ of $CaCl_2 \cdot 6H_2O$, 5.44 $mg \cdot l^{-1}$ of KH_2PO_4, 12.2 $mg \cdot l^{-1}$ of K_2HPO_4, 5 $mg \cdot l^{-1}$ of $FeCl_3$, 20 $mg \cdot l^{-1}$ of disodium EDTA, 0.03 $ml \cdot l^{-1}$ of HCl. From a stock solution, we added 1 $ml \cdot l^{-1}$ of trace elements resulting in concentrations of 10 $mg \cdot l^{-1}$ of disodium EDTA, 0.2 $mg \cdot l^{-1}$ of $ZnSO_4 \cdot 7H_2O$, 0.06 $mg \cdot l^{-1}$ of $MnCl_2 \cdot 4H_2O$, 0.6 $mg \cdot l^{-1}$ of H_3BO_3, 0.06 $mg \cdot l^{-1}$ of $Na_2MoO_4 \cdot 2H_2O$, 4 $mg \cdot l^{-1}$ of $FeSO_4 \cdot 7H_2O$, 0.04 $mg \cdot l^{-1}$ of $NiCl_2 \cdot 6H_2O$, 0.4 $mg \cdot l^{-1}$ of $CoCl_2 \cdot 6H_2O$, and 0.02 $mg \cdot l^{-1}$ of $CuSO_4 \cdot 5H_2O$.

Methanotrophic enrichment

Methanotrophs were enriched under batch conditions from municipal activated sludge from the wastewater treatment plant in Narbonne, France. We used 160 ml serum bottles with 50 ml as liquid volume of the media. To the media, 10 ml of inoculum were added so that a 100 ml gaseous headspace remained. Replicated enrichments (4-10 replicates) were incubated either with or without mixing using magnetic stirring. We also enriched the activated sludge mixed with fresh oxygenic photogranules, and oxygenic photogranules only without mixing.

For all enrichments, the serum bottles were sealed with rubber stoppers and capped using aluminum crimp caps. The headspace gas was mixed prior to the gas injection by combining 30 vol % CH_4 and 70 vol-% O_2. During the injection, a pressure of 1.49±0.05 bar (±standard deviation) was achieved in the serum bottle headspace. The pressure was manually confirmed using a handheld manometer (Keller Leo 2, Switzerland). We used purified methane for feeding from biogas produced in two laboratory-scale anaerobic digesters. This was done using a CO_2-absorbing bubble column containing NaOH at 3 M. The final methane concentration was on average 98.1±2.3% (±standard deviation). Pure oxygen was used.

The serum bottles were incubated at room temperature. Using a serological pipette, a volume of 20 ml of the methanotroph enrichment culture was transferred every five to seven days into a new serum bottle containing 40 ml of fresh media. After each transfer, the headspace was renewed with a fresh CH_4 and O_2 mixture (30%/70%) at approximately 1.5 bar. After a third transfer, i.e., after about 21 days, we observed decreasing oxygen and methane concentrations in the headspace of several bottles. From that point on, in all bottles, a mix of methane and oxygen (30%/70%) was added on a daily basis. After the fourth transfer, we harvested the enriched suspended methanotrophic cultures and transferred them to five new serum bottles with fresh media and approximately ten oxygenic photogranules, each, with an approximate average diameter of 1-2 mm. The untreated, fresh oxygenic photogranules were obtained from a continuously operated reactor. To the methanotroph enrichment and oxygenic photogranules, we added 100% methane in the headspace, assuming that oxygen would be provided by photosynthesis. Bottles were incubated on a shaker that was equipped with fluorescent light bulbs providing photoactive radiation (PAR) at approximately 58 $\mu mol \cdot m^{-2} \cdot s^{-1}$. PAR was measured at the outside of the flasks using a light meter LI-250A (LI-COR, USA). After one week, the active methanotrophic photogranules were separated from the suspended biomass and rinsed. Photogranules were rinsed using deionized water before the final transfer into the continuous reactor to avoid

suspended and loosely attached biomass. Only the solid photogranule biomass was used to inoculate the continuous reactor.

Set-up and operation of continuous reactor

Approximately 60 active methanotrophic photogranules were transferred to an airtight glass vessel with 1.8 l of liquid volume, operated as a continuously stirred tank reactor. Fig. 1 shows a schematic view of the reactor set-up. We used overhead mixing as this type of agitation does not impact photogranules stability. The use of magnetic stir bar resulted in gradually crushing photogranules (Milferstedt et al., 2017). We used an airtight overhead magnetic stirrer head of the g-mrk ptfe type with a ground joint (Bola Bohlender GmbH, Germany), connected to an overhead motor using a polyoxymethylene globe stirrer coupling (Bola Bohlender GmbH, Germany). The coupling compensates potential misalignment between the overhead motor and the magnetic stirrer head. The reactor vessel was a borosilicate glass beaker with a glass flat flange lid containing one central and three angled ground necks.

Mixing was provided by a stainless-steel impeller operated at 100 rpm during the first 30 days of reactor operation, increased to 125-128 rpm on day 31 for the remainder of the experiment. Light was provided using standard 60 × 60 cm^2 LED panels emitting warm white at 4000K. A light intensity of approximately 45 $\mu mol \cdot m^{-2} \cdot s^{-1}$ PAR was measured at the outside of the vertical reactor surface. The reactor was operated at an average room temperature of 23.2±1.0°C (±standard deviation) without active temperature control. The dissolved oxygen concentration in the reactor fluctuated with an average 1.8±3.2 $mg \cdot l^{-1}$. High oxygen concentrations were observed to be a consequence of membrane fouling of the electrode membrane. The average pH in the reactor was 7.0±0.2.

Initially, all headspace compartments and the experimental set-up (e.g., tubings, fittings) were flushed with nitrogen and methane (92/8 vol/vol) before the start of operation. As the supply of biogenic purified methane was limited, pure nitrogen (100%) was used for flushing the headspace during routine reactor operation, e.g., after manual interventions for cleaning and biomass removal. After start-up, methane-saturated feed was continuously pumped into the reactor. The reactor was operated at a hydraulic retention time of 12 h. The media contained on average 17.6±2.2 mg $CH_4 \cdot l^{-1}$ (±standard deviation) and the volumetric organic loading rate was approximately 35.1±4.5 mg $CH_4 \cdot l^{-1} \cdot d^{-1}$.

Media preparation

As mentioned in section 2.1, the initial media composition for the continuously operated reactor was identical with the batch experiments. Media was prepared in an O_2- and CO_2-free closed atmosphere obtained by initially sparging the preparation system with nitrogen gas for approximately 15 min until the dissolved oxygen concentration measured with a handheld oxygen meter (Multi 3620 IDS, WTW, Germany) was below the detection limit. This precaution was taken to limit the supply with externally provided CO_2 and oxygen, so that growth of methanotrophs and phototrophs in the reactor could be linked to their respective metabolic activities. Then, the media was saturated with purified methane by recirculating methane through the solution using a diaphragm pump and porous diffusors. This step took around six hours. The media was then transferred using gas-tight tubing and a peristaltic pump into the 20 l media storage tank. A capacity of 20 l ensured autonomy for a 72 h period. Media preparation and media storage were physically separated in two bottles to assure continuous feeding during media preparation. One batch of methane saturated media had a maximum volume of 10 l, limited by laboratory safety consideration. The long preparation was mostly due to slow gas transfer from the methane atmosphere to the aqueous phase.

Photogranule size analysis

We quantified the total number of all photogranules in the reactor and their size distribution based on equivalent diameters. For this, we temporarily placed the entire content of the reactor on a custom-built square tray with a transparent glass bottom (17.7 × 17.6 cm^2) that was then placed on the glass surface of a desktop scanner (Canon LiDE 220, Japan). An image of the photogranules through the bottom of the tray was acquired with the dimensions of 5583 × 5556 pixels and saved as a non-compressed 8-bit gray-level tagged image format (tif) file. Care was taken to avoid overlap or contact between individual photogranules as this would have made the subsequent image analysis more complicated. With increasing numbers of photogranules in the reactor, photogranules were partitioned into several batches and multiple images were acquired. Using a custom-made script in ImageJ (Schneider et al., 2012), we then used the maximum entropy thresholding algorithm to differentiate photogranules from the background. Using the MorphoLibj plugin (Legland et al., 2016), noise was removed on the images by applying the morphological operation "opening" with a radius of 1. White pixels within apparent particles on the images were filled using the "fill holes" command. Particles in contact with the image boundaries

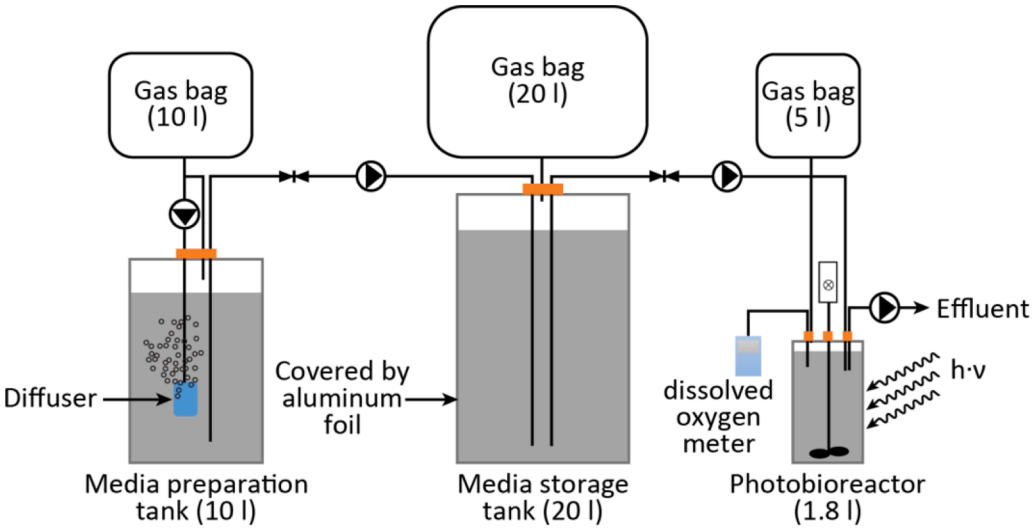

Fig. 1. Presentation of the continuous reactor set-up. The gas bag connected to the media preparation tank was used as methane reservoir during the preparation of methane-saturated batches of media. The finished media batches were transferred to the media storage tank, from where it was continuously pumped into the reactor. The gas bag connected to media storage equilibrated pressure changes resulting from filling and emptying the tank. The gas bag connected to the reactor equilibrated potential pressure changes in the reactor.

were removed using the "kill borders" command to avoid counting particles that were not entirely visible on the images. The area of each detected object was then quantified and translated into the equivalent diameter of an assumed perfect circle with the same area.

Analytical methods

Gaseous samples were withdrawn from the headspace of enrichment cultures and the reactor using gas-tight syringes (SGE-Europe). Subsequently, samples were analyzed using gas chromatography (Perkin Elmer GC580, USA) for determination the concentration of CH_4, N_2, CO_2 and O_2. The GC was equipped with a thermal conductivity detector (RT-Msieve 5A column, 0.32 mm diameter, 30 m length and 30 μm film). Helium was used as the carrier gas at a flow rate of 35.4 $ml \cdot min^{-1}$. The oven temperature was 60°C. Dissolved methane was determined by converting the dissolved COD measurement by multiplying with the specific COD equivalent of methane: 4 g $COD \cdot g\ CH_4^{-1}$. Total and dissolved COD were determined daily using standard COD test kits with a detection range of 0-150 $mg \cdot l^{-1}$ (Aqualytic, Germany). The influent and effluent samples were withdrawn using a 5 ml syringe containing no gas phases.The samples were immediately and directly filtered through a 0.45 μm PTFE hydrophilic membrane syringe filter into a COD test kit and sealed immediately. Speedy sample handling and processing ensured reliable measurements of dissolved methane. Total COD measurement was conducted without filtering the sample. We compensated for any background COD by measuring blank COD concentrations in the ready-made media before methane equilibration, and then subtract that from all consecutive COD measurements made at the reactor inlet and outlet. COD compensation was done to account for any compounds in the media with a potential contribution to COD, notably EDTA. Total suspended solid (TSS) was measured following standard methods 2540D after the filtered samples (Pre-weighted Glass Fiber Filter, pore size 0.45 μm, diameter 47 mm, 934-AH RTU, Whatman, UK) dried at 105°C for 1 h (Rice et al., 2013). Samples were taken in duplicates for each gas, COD and TSS measurement.

Observed biomass yield

The overall observed biomass yield was determined based on the ratio of cumulative generated biomass (g TSS) per cumulative consumed substrate (g CH_4). Assuming 15% inorganic biomass fraction, the cumulative generated biomass in the unit of g TSS is converted to the unit of g VSS. The consumed substrate (g CH_4) was measured daily as COD removed by the system. The cumulative generated biomass consists of the accumulated biomass in the system, cumulative biomass wastage, and biomass effluent. The accumulated biomass and biomass wastage were measured weekly while doing cleaning and maintenance. In addition, the suspended biomass in the effluent was measured daily. We calculated the specific COD of TSS using linear-regression analysis (Chon et al., 2011).

Dependence of methanotrophic activity on photogranules size

When assuming phototropic methane conversion to be a surface-depending process, photogranule size may influence the specific phototrophic and methanotrophic activities by affecting surface to volume ratios and diffusional lengths. We analyzed the specific metabolic activity in batch experiments in serum bottles under the same conditions as during the enrichment experiments. We prepared a serum bottle per size class containing on average six similar-sized photogranules. Photogranules were sampled during stable reactor performance on day 29, 57, 72, 79, 86, and 97. For each test, three size classes, 1.0–2.2 mm, 2.3–3.7 mm, and 3.8–5.5 mm, were defined.

Microbial analysis

Photogranules were sampled for community analysis (1) before contact with methanotrophic enrichments (samples named 'background'), (2) after incubation with methanotrophic enrichments (samples named 'inoculum') and (3) during continuous operation of the reactor (samples named 'continuous reactor operation'). Sampled photogranules were stored at −20°C for subsequent DNA extraction. DNA was extracted using the DNeasy PowerWater Kit (Qiagen, Germany), according to the manufacturer's instructions. The genomic DNA was used in two independent MiSeq sequencing reactions for 16S rRNA amplicons and 23S rRNA amplicons.

The 16S rRNA amplicons were generated using the primer pair 515F (5'-GTGYCAGCMGCCGCGGTA-3') and 928R (5'-CCCCGYCAATTCMTTTRAGT-3') (Wang & Qian, 2009) plus their respective linkers. The primers target the V4-V5 hypervariable regions of the 16S rRNA gene. They amplify most of the bacterial and archaeal known diversity. The PCR mixtures (50 μl) contained 0.5 U of MTP™ Taq DNA Polymerase (Sigma-Aldrich, Germany) with its corresponding buffer, 200 mM of each dNTP, 0.5 mM of each primer, and 10 ng of genomic DNA. Reactions were performed in a Mastercycler thermal cycler (Eppendorf, Germany) as follows: 95°C for 2 min, followed by 30 cycles of 95°C for 1 min, 65°C for 1 min, and 72°C for 1 min, with a final extension at 72°C for 10 min.

The 23S rRNA amplicons were generated using the primers pair p23SrV_f1 (5′-GGACAGAAAGACCCTATGAA-3′) and p23SrV_r1 (5′-TCAGCCTGTTATCCCTAGAG-3′) (Sherwood & Presting, 2007) plus their respective linkers. This primer pair targets a region in the 23S rRNA of cyanobacteria and plastids in algae. The 50 μl PCR mixtures contained 0.5 U of MTP™ Taq DNA Polymerase (Sigma-Aldrich, Germany) with its corresponding buffer, 200 mM of each dNTP, 0.3 mM of each primer, and 10 ng of genomic DNA. Reactions were performed in a Mastercycler thermal cycler (Eppendorf, Germany) as follows: 94°C for 2 min, followed by 30 cycles of 94°C for 20 s, 59°C for 30 s, and 72°C for 30 s, with a final extension at 72°C for 10 min. The respective lengths of the PCR products were quality-checked using a Bioanalyzer 2100 (Agilent, USA).

In a second PCR of 12 cycles, an index sequence was added, and the resulting PCR products were purified and loaded onto the Illumina MiSeq cartridge according to the manufacturer's instructions for sequencing of paired 300 bp reads (v3 chemistry). Library preparation and sequencing was done at the GeT PlaGe Sequencing Center of the Genotoul Lifescience Network in Toulouse, France (https://get.genotoul.fr/). The datasets for this study can be found in the NCBI Sequence Read Archive (SRA) database as Bioproject PRJNA686893.

Sequences were dereplicated, quality checked, chimera checked and affiliated with a taxonomic description using Mothur version 1.42.3 (Schloss et al., 2009). Sequence treatment included preclustering at four differences in nucleotides over the length of the amplicon and chimera checking using uchime (Edgar et al., 2011). We removed all sequences that appeared less than three times in the entire dataset. The databases SILVA (Quast et al., 2013) 132 SSU (16S rRNA) and 132 LSURef (23S rRNA) were used for alignment and as taxonomic outline.

Cleaned up and taxonomically affiliated sequence data was written into a biom file and was subsequently merged with the environmental data and analyzed in R version 4.0.3 (R Core Team, 2020) using the R packages phyloseq (McMurdie & Holmes, 2013) and tidyverse (Wickham et al., 2019). For the 16S rRNA amplicons, we removed the sequences affiliated with cyanobacteria using subset_sample command in phyloseq with the argument !(Phylum == "Cyanobacteria"). For the 23S data, we separated the chloroplast sequences from cyanobacteria using the same command with the argument (Phylum == "Cyanobacteria" & ! (Order=="Chloroplast")).

On average, the 16S rRNA amplicons contained 50600±7300 (±standard deviation) bacterial sequences per sample, of which on average 17100±7500 were not cyanobacteria. Even though the 16S

rRNA reverse primer supposedly excludes cyanobacterial sequences (Hodkinson & Lutzoni, 2009), we nevertheless find them in high abundance, likely because of the overwhelming presence of cyanobacteria in the systems, with the exception of the activated sludge sample that only contained four sequences affiliated with phototrophs in the 16S amplicon. On average, the 23S rRNA amplicons contained 51700±6700 sequences per sample, of which on average 1800±1600 or 3.5±3.0% were eukaryotic microalgae. The counts disregard the activated sludge sample that only contained 370 sequences affiliated with cyanobacteria in the 23S amplicon, however, in which we detected the highest absolute and relative counts of microalgae in this study.

Based on taxonomic outlines offered by the SILVA 132 SSU and LSU databases, we considered the following taxa detected in our amplicons as putative methanotrophic: the families Methylococcaceae (containing the genus *Methyloparacoccus*), Methylomonaceae (containing the genera *Methylomonas, Methylobacter, Methylomicrobium*, and *Methylosarcina*), and Beijerinckiaceae (containing *Methylocystis* and *Methylobacterium*). We considered as non-methanotrophic methylotrophs the genus *Methyloversatilis* of the family Rhodocyclaceae and the family Methylophilaceae (containing the genera *Methylophilus* and *Methylobacillus*).

Results and Discussions

Successful establishment of a syntrophic, methane-degrading community

Methanotrophs were enriched from activated sludge in gas-tight, stoppered serum bottles with a mixture of oxygen and methane in the headspace. We tested enrichments with and without mixing by magnetic stirring. After four transfers every five days into fresh media, all enrichments that were mixed during incubation removed methane and produced carbon dioxide according to the methane oxidation stoichiometry, closing the mass balance by more than 80%. We detected methane removal in approximately half of statically incubated cultures (i.e., without mixing). Mixing increases methane transfer across the gas-liquid interface, leading to more successful incubations. The enrichments from unstirred oxygenic photogranules mixed with activated sludge removed methane. However, unstirred and stirred activated sludge enrichments removed methane twice and four times faster, respectively. Fresh photogranules did not exhibit a measurable methanotrophic activity.

We detected methane removal after adding 100% methane without externally provided oxygen to a mixture of fresh, non-methanotrophic photogranules and methanotrophic enrichments from activated sludge. Also, the production of oxygen and CO_2 was measured. This observation demonstrated the onset of engineered syntrophic interactions between methanotrophs and oxygenic photogranules. We were thus able to introduce a novel function into an existing, granulated microbial ecosystem, laying the basis for a potential future application in biotechnology in which biomass harvesting is feasible.

Continuous reactor performance for removing dissolved methane

The ecologically engineered methane-converting photogranules were then used as inoculum for the continuously operated reactor. Fig. 2 shows the dissolved COD removal efficiency as proxy for methane removal as well as effluent total suspended solids (TSS) over time. Dissolved methane removal efficiencies fluctuated over the first week of operation. Effluent concentrations stabilized over the following two weeks and the methane removal efficiency steadily increased. On day 16, biofilm on reactor surfaces and equipment was removed, resulting in a 5% decrease in methane removal. The rather moderate decrement indicates that the vast majority of methane oxidation was situated in photogranular biomass and not in the biofilm formed on the reactor surfaces. Approximately 10 mg TSS·l^{-1} of suspended solids were washed out from the reactor. Photogranules became increasingly more filamentous at this time (Fig. 3a, middle). The change of photogranule morphology could have been influenced by the increase in biomass concentration and a local decrease in light availability in the reactor. The cyanobacteria might try to increase their surface area by forming filamentous outgrowth and therefore exposure to light (Biddanda et al., 2015).

After about three weeks of operation, effluent TSS increased due to the detachment of filaments from the photogranules. Application of higher mixing intensity on day 31 from 100 rpm to 125-128 rpm resulted in an increase in methane removal efficiency, now exceeding 90%. Mixing serves the purposes of minimizing the laminar boundary layer around the photogranules and keeping the photogranules in suspension (Beun et al., 2000; Liu et al., 2003). We also changed mixing to

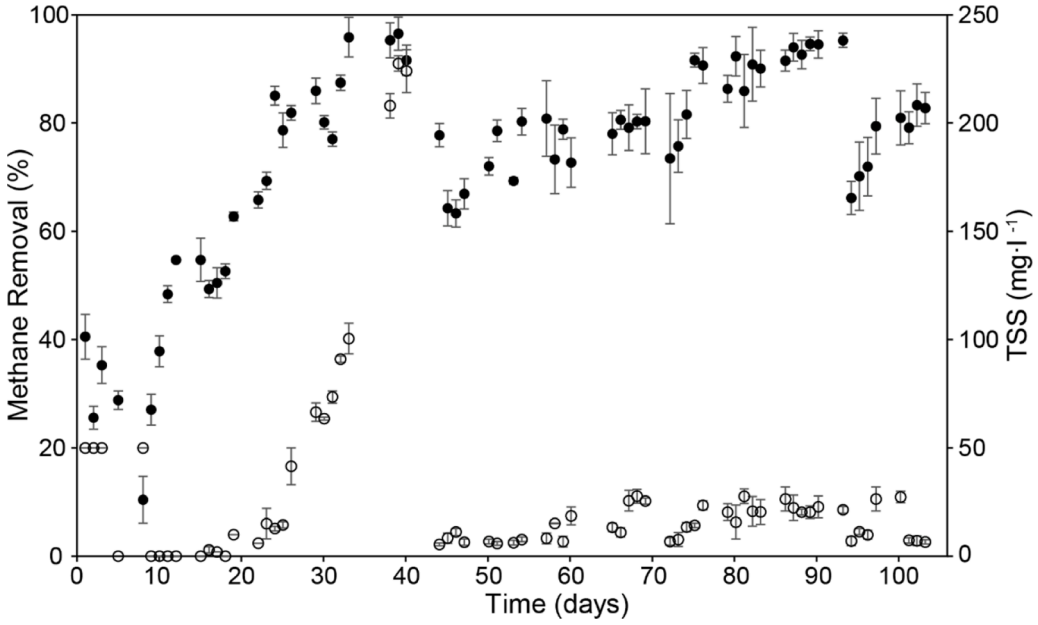

Fig. 2. Removal efficiency of dissolved methane (filled circles) and concentrations of total suspended solids in the effluent (TSS, open circles) during continuous reactor operation. Mixing speed was increased on day 31. On day 40, the reactor effluent clogged. Severe biomass washout occurred on days 43 (deliberate) and 94 (accidental).

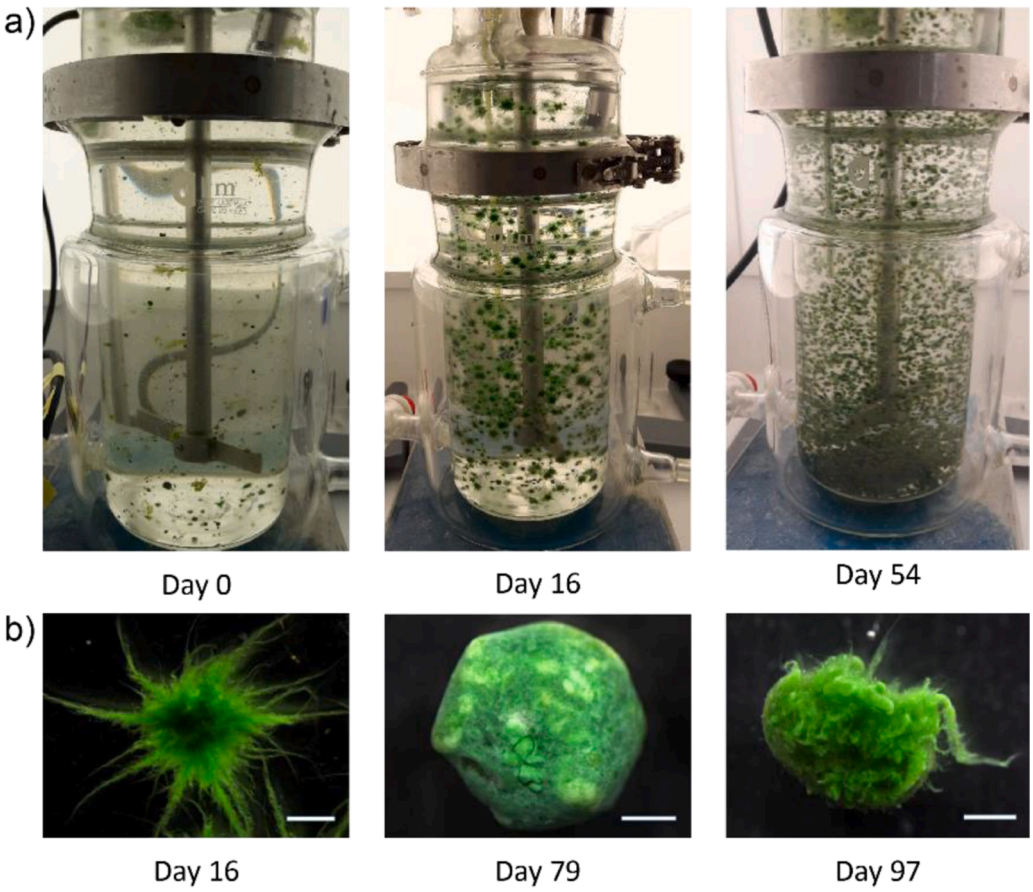

Fig. 3. Photogranule development on macro and micro-scale. a) Full views of the reactor vessel. b) Examples of typical photogranule morphologies during continuous operation. Images were taken using white-light stereomicroscopy (scale bar for all images is 1 mm).

increase detachment of filaments from the photogranule surfaces. This approach worked, resulting in temporarily increased effluent suspended solid concentrations from the reactor (Fig. 2, days 31 to 40) and less filamentous photogranules. However, the sudden detachment became problematic for reactor operation at day 40 when the effluent clogged, turning operation into safety mode for two days, i.e., without water in and outflow. The reactor was operational again after cleaning and wasting some photogranules at day 43.

On day 43, biomass was purposely wasted to obtain approximately 1.5 g TSS·l^{-1}. Introduction of a weekly cleaning and biomass wasting protocol, by removing approximately 0.5-0.7 g TSS·l^{-1}, prevented further clogging and maintained a balanced biomass concentration in the reactor of approximately 1.2 g TSS·l^{-1}. This weekly biomass removal represented about one third to half of the biomass in the reactor. The removal of granular biomass on day 43 caused a drop in methane removal efficiency from about 90% to 60%. The removal efficiency reached on average 84.8±7.4% (±standard deviation) between day 54-93. On day 94, a decreased methane removal efficiency was observed due to accidental wasting of a large numbers of photogranules. However, performance recovered over the next week to above 80%. The average effluent concentration of dissolved methane and the averaged methane removal rate during reactor operation was 4.9±3.7 mg CH_4·l^{-1} and 26.3±2.6 mg CH_4·l^{-1}·d^{-1}, respectively. In van der Ha et al. (2011), an overall methane oxidation rate was reported to be 171 mg CH_4·l^{-1} liquid phase·d^{-1} which appears to be 6.6 times higher than in our experiments. A major factor leading to a higher removal rate is the organic loading. In van der Ha et al. (2011), 235 ml of CH_4 were added over 72 hours, which corresponds to approximately 258 mg CH_4·l^{-1}·d^{-1} at 22°C. Our OLR of 35.1±4.5 mg CH_4·l^{-1}·d^{-1} was thus, 7.3 times lower. It is important to note that the rates are not immediately comparable as van der Ha et al. (2011) worked in a batch system over 90 h, while our results are obtained in a CSTR with an HRT of 12 h.

The observed overall biomass yield was 0.7 g TSS·g COD^{-1}, equivalent to 0.6 g VSS·g COD^{-1} (assuming 15 % inorganic biomass fraction). Per mass substrate (CH_4) this is equivalent to 2.4 g VSS·g CH_4^{-1}. The observed yield represents the combination of cellular yield from methanotrophic and cyanobacterial growth. Literature values of methanotrophic yields relevant for our study have been reported by Leak & Dalton (1986) and Arcangeli & Arvin, (1999). By theoretical analysis and experimental observations on suspended Methylococcus capsulatus, Leak & Dalton (1986) reported cellular yield of 0.6-0.7 g VSS·g CH_4^{-1} on cultivation conditions similar to this study. Arcangeli & Arvin (1999) studied a methanotrophic biofilm enriched from landfill soil and estimated the dry weight yield to be 0.56 g VSS·g CH_4^{-1}. As conditions and growth technique, granular aggregation is similar to biofilms, and our media (0.02 mg·l^{-1} of $CuSO_4 \cdot 5H_2O$) was comparable to the Cu limited experiment of Leak and Dalton (1986), we estimate methanotrophic yields to be in the order of 0.5-0.6 g VSS·g CH_4^{-1}, which leaves the remaining observed 1.8 g VSS·g CH_4^{-1} to be the autotrophic contribution. Assuming all CO_2 from the mineralization of methane to be assimilated by the phototrophic bacteria, a combined methanotrophic and phototrophic yield of 1.54 g VSS·g CH_4^{-1} would be theoretically possible. The observed combined yield (2.4 g VSS·g CH_4^{-1}) therefore indicates an additional autotrophic growth contribution of 0.9 g VSS·g CH_4^{-1} probably originating from the inlet bicarbonate. High biomass yields in this system highlight the potential for the recovery of chemical energy or the methane-based biorefinery using photogranules. The overall COD balance closed at 91% of the inlet COD. The unaccounted 9% COD could be explained the reactor system still not completely at steady state (positive bioaccumulation), and by the negative COD

contribution by phototrophically produced oxygen consumed by the methanotrophs during methane mineralization.

We can rule out leakages in the system and therefore potential methane loss or oxygen and CO_2 entering the system. The tightness of the reactor system was verified by frequently checking the gas composition in the headspace of the reactor using gas chromatography. The results showed that in the headspace, the dominant gas were nitrogen, oxygen, and methane by 89.3±3.3%, 4.4±2.6%, and 4.9±2.3% (v/v) (±standard deviation), respectively. The high presence of nitrogen gas resulted from the regular flushing of the headspace with nitrogen during reactor cleaning and maintenance. Only at most traces of CO_2 were detected in the gas phase at 0.01±0.02% (v/v).

Cyanobacteria can use CO_2, HCO_3^- and possibly also CO_3^{2-} as carbon source (Schneider & Campion-Alsumard, 1999). In our study, methane was not the sole carbon sources, but HCO_3^- was contained as hardness in the tap water we used for media preparation. Based on the growth stoichiometry for methane oxidation coupled to photosynthesis, the theoretically produced oxygen from CO_2 assimilation during photosynthesis only provides roughly 20% of the oxygen needed for complete methane oxidation. The presence of HCO_3^- to the media would enhance the methane removal efficiency due to higher oxygen availability from bicarbonate photosynthesis. The 4 mM HCO_3^- contained in the tap water could theoretically supply an additional 2.58 mM O_2, or an equivalent COD of 82 $mg \cdot l^{-1}$, upon autotrophic growth. Hence, methane oxidation is not stoichiometric oxygen limited by cyanobacterial growth. Similar findings were reported in the literature where in the absence of external oxygen supply, microalgal photosynthesis was not sufficient for methane oxidation (Bahr et al., 2011). Only when bicarbonate was introduced, the methane removal efficiency increased.

We suggest that the elevated methane removal in the absence of any external oxygen supply can only be explained by in-situ oxygen production and immediate uptake by methanotrophs. Our results therefore demonstrate the establishment of syntrophic interactions between phototrophs and methanotrophs. This syntrophy was stably maintained over seven weeks during continuous reactor operation.

Photogranule development in continuously operated reactor

During continuous reactor operation, new photogranules rapidly formed (Fig. 3). After 16 days of continuous operation, the photogranules became dark green, roughly spherical, and filamentous (Fig. 3). The presence of filamentous cyanobacteria was confirmed by white-light and fluorescence microscopy. Development of the filamentous morphology likely caused the increase in suspended solids in the reactor effluent (Fig. 2). We successfully generated a less filamentous photogranule phenotype by increasing mixing from 100 rpm to 125-128 rpm starting on day 31. Immediately after the increase, the photogranules lost substantial amounts of filaments. Whitish areas on the photogranules surface became visible (Fig. 3b, middle).

Using image analysis, we determined the number and the size of photogranules in the reactor. Over the first four weeks, the number of photogranules increased from initially 60 with an approximated total surface area of 0.08 cm^2 (day 0), to 888 and a total surface area of 240 cm^2 on day 16, and to about 2000 with a total surface area of 551 cm^2 on day 29 (Fig. 4). After the major wasting and cleaning event on day 43, the number and surface area of photogranules decreased to 613 and 77.3 cm^2, respectively. However, the biomass concentration increased in the following days and reached more than 3500 photogranules and 1105 cm^2 of surface area on day 79 (Fig. 4).

The range of biomass diameters on day 16 was between 1 and 7 mm, with an average of 2.6±1.3 mm (±standard deviation). On day 43, because of increasing shear, the predominant diameter of photogranules was less than 2 mm. The largest size of photogranules in the reactor was approximately 7.5 mm. This size is larger than the typical size of aerobic granular sludge with sizes in the range of 4 to 6 mm (Beun et al., 2000; Morgenroth et al., 1997). However, towards the end of reactor operation, more than 90% of the photogranules were between 1 and 3 mm with an average diameter of 2.6±1.0 mm. This value is greater than the size of photogranules (≤2 mm in diameter) reported from previous photogranule reactor studies (Abouhend et al., 2018; Liu et al., 2017).

Size specific analysis of methanotrophic activity

Photogranule size may influence the specific phototrophic and methanotrophic activities as we assume phototrophic methane conversion to be a surface-depending process. Photogranule size affects the surface to volume ratios and diffusional lengths. We analyzed the specific metabolic activity in batch experiments for sets of on average six similar-sized photogranules in size classes between 1.3 and 5.5 mm in average diameter (Fig. 5). Photogranules were sampled during stable reactor performance. Photogranules with diameters of approximately 1-2 mm gave the highest surface-specific methane removal rate of 0.53±0.02 mg $CH_4 \cdot d^{-1} \cdot mm^{-2}$ (±standard deviation). The methane removal rate per photogranule surface area decreased with increasing diameter (Fig. 5a). The relation with the surface to volume ratio is presented in Fig. 5b. An elevated surface to volume ratio is beneficial for

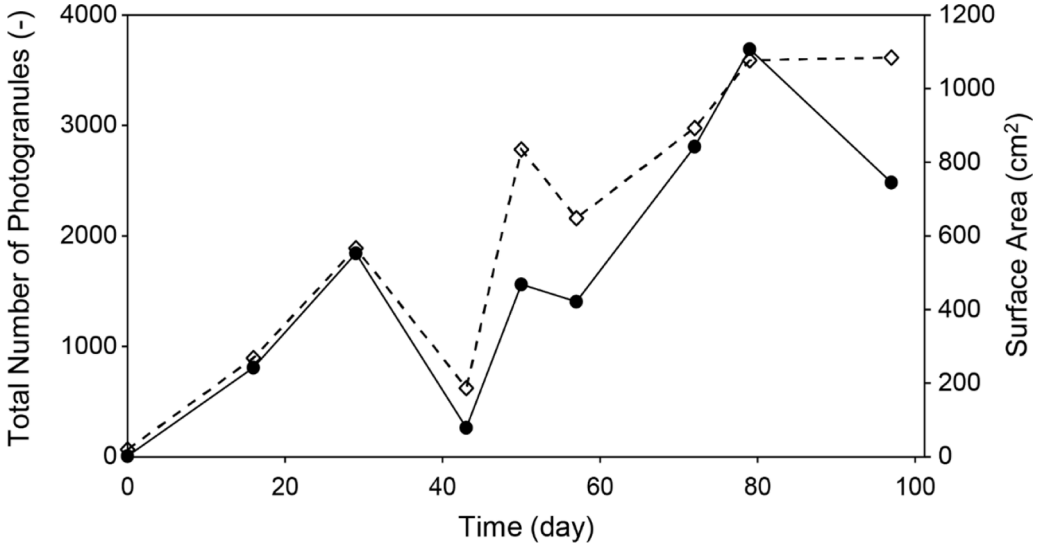

Fig. 4. The total number (empty diamonds) and surface area of photogranules (filled circles) in the reactor during continuous operation.

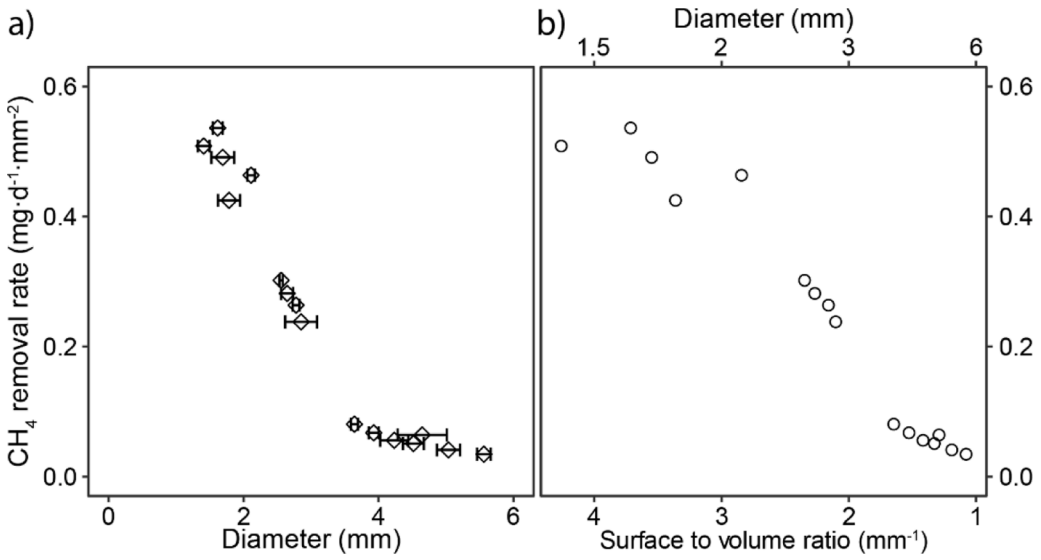

Fig. 5. Surface specific methane removal rates for individual photogranule sizes. Rates are plotted by (a) the average diameter of the photogranule batch, and (b) by the surface to volume ratio, derived from the average diameters of the tested photogranules. Each point represents an independent batch experiment conducted with on average six similar-sized photogranules.

methane removal. From a conversion perspective, it is favorable to engineer a size distribution within the reactor of minimal photogranule diameter. The surface dependent character of photogranule metabolism was also shown in a recent study by Abouhend et al. (2020) in which oxygenic photogranules of 0.5−1.7 mm in diameter showed the highest oxygen production rate compared to bigger photogranules (Abouhend et al., 2020). Higher oxygen production rates influence the treatment potential of the biomass, in this case dissolved methane removal, due to higher oxygen availability from photosynthesis as electron acceptor. Bigger photogranules may also become less active because they lose their cyanobacteria from the core as the photo-layer appear to be limited to depth of about 700 μm (Milferstedt et al., 2017).

Community analysis related to methane removal performances

Using MiSeq amplicon sequencing, we analyzed the microbial communities in various photogranules sampled from the sequencing batch reactor, as well as the enriched inoculum and background material before the enrichment. We detected the presence of sequences belonging to methylotrophic bacteria in our samples (Fig. 6a). The detected methylotrophs predominantly belong to methanotrophic bacteria, a subgroup of the methylotrophs, able to directly use methane as carbon

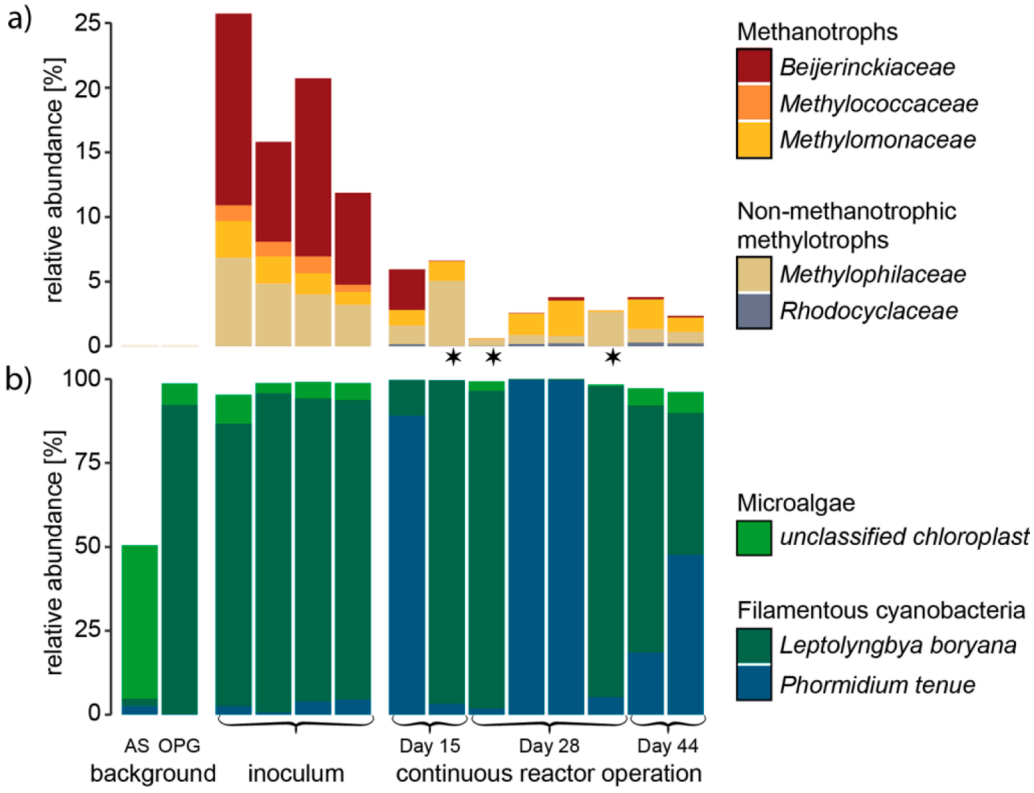

Fig. 6. Relative abundances of methylotrophic and phototrophic taxa in photogranules and background material. The background material before the enrichment is the original activated sludge (AS), and an oxygenic photogranules (OPG). The inoculum after the enrichment process is represented by four photogranules. In total eight photogranule communities during continuous reactor operation are shown for days 15, 28 and 44. a) Putative methylotrophic bacteria (Silva SSU 132) among the non-phototrophic bacteria, i.e., excluding cyanobacteria, in the 16S rRNA amplicons. The three samples with asterisks mark photogranules in which methanotrophs are present in low abundances compared to non-methanotrophic methylotrophs. b) Major (>5% total abundance) cyanobacterial and chloroplast OTUs (Silva LSU 132) among the phototrophic taxa of the 23S rRNA amplicons.

and energy source. A frequent intermediate or even final product of methanotrophs is methanol (Kalyuzhnaya & Xing, 2018). Also, non-methanotrophic methylotrophs were detected in elevated abundances (Fig. 6a), notably of the family *Methylophilaceae*, often involved in methanol conversion (Yu et al., 2017). These groups of bacteria may participate in a communal metabolism of methane (Beck et al., 2013; Oshkin et al., 2015).

In the background material before the enrichment process, only in raw activated sludge, we detected sequences of one methanotrophic type in the 16S rRNA amplicons at a relative abundance of 0.02% of all bacterial sequences (excluding cyanobacteria). This sequence type was unique to the activated sludge sample and undetected in the inoculum and during reactor operation. In oxygenic photogranules, no sequences affiliated with known methanotrophic bacteria were detected (Fig. 6a, "background"). The activated sludge and oxygenic photogranules used as starting material in this study contained fewer sequences of methanotrophic bacteria than previous observations (Milferstedt et al., 2017). Non-methanotrophic methylotrophs were undetectable in background activated sludge and oxygenic photogranules.

The enrichment process had a profound impact on the microbial community as at the end of it, 18.5±6.0% (±standard deviation) of all non-cyanobacterial bacterial 16S rRNA sequences were affiliated with known methylotrophic bacterial genera (Fig. 6a, "inoculum"). Of this methylotrophic fraction, 74.1±4.8% were known methanotrophs, notably of the family of *Beijerinckiaceae*. These bacteria are Alphaproteobacteria, frequently described as type II methanotrophs. Across all samples containing sequences of methanotrophic *Beijerinckiaceae*, 98.5±4.5% were of the genus *Methylocystis*. *Methylocystis* are often considered versatile in their oxygen and methane requirements (Knief, 2015) allowing them to thrive in ecosystems with a varying methane supply (Knief, 2015). This survival strategy is believed to be linked to the presence of two variants of particulate methane monooxygenase A (PmoA) (Knief, 2015), the key enzyme in methane oxidation, converting methane to the intermediate methanol. One of them is especially adapted to low methane to oxygen ratios in the feed, as likely encountered during batch feeding cycles in the enrichment process. The batch supply of methane and oxygen may thus be a key environmental factor favoring growth of these methanotrophs whereas the continuous exposure to methane at low concentrations as in the continuously fed reactor may promote others.

Also present at the end of the enrichment, however, at notably lower abundances of 21.6±5.5% (±standard deviation) of all methanotrophic bacteria, were members of the families of *Methylococcaceae* and *Methylomonaceae*. These subdominant families belong to the Gammaproteobacteria, also known as type I methanotrophs. Traditionally, the distinction in type I and type II methanotrophs allowed the differentiation of mutually exclusive physiological traits. Over the last years, however, it was realized that the distribution of these traits was less exclusive, and the distinction has become less meaningful (Dedysh & Knief, 2018).

During photoreactor operation, the overall relative abundance of methylotrophs dropped from 18.5% in the inoculum to, on average, 3.5±2.0% (±standard deviation), of which roughly half of all sequences were known methanotrophs (1.8±1.4%). Most analyzed photogranules had an approximate diameter of 2 mm and thus a comparable biovolume, with the exception of the third and fourth samples on day 28 that had a diameter of 5 mm. Assuming an approximately constant microbial community size for equally sized photogranules, the observed relative changes in the microbial community are likely translated into an absolute decrease in abundance per photogranule. Most of this loss is attributed to a significant decrease in the methanotroph *Methylocystis* of the *Beijerinckiaceae* (t-test, p-value = 0.006). Also, the abundance of the other two methanotrophic families *Methylococcaceae* and *Methylomonaceae* decreased significantly (t-test, p-value = 0.02) dropping from, on average, 2.9±1.0% to 1.3±0.9%. After the disappearance of the *Methylocystis*, these two families presented the majority of methanotroph-affiliated sequences during reactor operation (87.2±24.2%, Fig. 6 "continuous reactor operation"). Two photogranules, sampled at day 28, only contained about 0.1% of methanotrophic sequences, more than ten times fewer than the other samples taken during reactor operation. The overall loss of methanotrophs may be explained by a reduced substrate availability per photogranule during reactor operation with the increasing number of photogranules in the system. The comparably low number of methanotrophs may thus be a steady state concentration adapted to the prevailing environmental conditions. Even though the drop in methanotrophs is significant, the abundance of methylotrophic bacteria, including methanotrophs remains about 100 times above the background levels before the enrichment. We note that the overall methanotrophic performance of the reactor system was maintained even at comparably low sequence abundances of 1.8±1.4% of methanotrophs.

We systematically detected sequences of non-methanotrophic methylotrophs in our amplicons, notably of the family *Methylophilaceae*. Their sequences represented on average 4.7±1.6% (±standard deviation) in the inoculum, and 1.7±1.5% during reactor operation. In natural systems like sediments, these organisms are frequently found to respire methanol produced by methanotrophic bacteria (Yu et al., 2017). Yu et al. (2017) even suggested that among non-methanotrophic methylotrophs and methanotrophs, specific non-random pairings exist that seem to possess an environmental advantage over others. We did not detect specific pairings in our data, but the abundances of *Methylophiliaceae* sequences appears to be roughly one third of the counts of known methanotrophic sequences in photogranules (linear regression through origin with slope of 0.345 and adj-r^2 of 0.74) (Fig. 7). The constant ratio in abundance between two distinct phylogenetic groups hints towards a stoichiometric relationship between the implied organisms, possibly through metabolite dependencies. In Fig. 7, notable exceptions to an otherwise strong linear relationship are two for the three samples marked with an asterisk in Fig. 6. In these samples, methanotrophs are only present at a comparably low number. The exceptions indicate that metabolic heterogeneity between photogranules existed in our reactor, with the coexistence of putatively methanotrophic and non-methanotrophic photogranules. The non-methanotrophic photogranules may consume substrates provided by other methanotrophic photogranules. These substrates could be for example methanol. A complete CH_4 to CO_2 conversion chain may therefore not be required to be present within each photogranule, but the entire population of photogranules participates in the methane

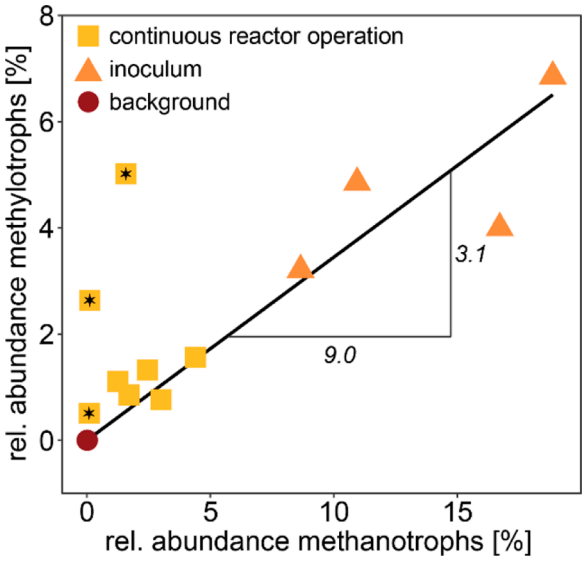

Fig. 7. Ratio of non-methanotrophic methylotrophs vs. methanotrophs sequence types in the 16S rRNA amplicons.

conversion, cross-feeding beyond the boundaries of individual photogranules.

The enrichment process and the consequent transfer into the continuously operated reactor also shaped the non-methylotrophic and non-phototrophic bacteria in the community. During the enrichment, *Sphingomonadaceae* were enrich and reach abundances in the non-phototrophic 16S rRNA amplicons of more than 45% in one photogranule. This organism was affiliated with *Porphyrobacter*, an organism believed to be involved in the recycling of organic matter. During reactor operation this organism became less abundant in most cases while other recyclers increased in abundance, notably *Chitinophagaceae*. Some of the detected organisms are facultative anaerobes, suggesting that there are anaerobic microhabitats within the photogranules. No apparent correlation with the dynamics that we observed for the methylotrophs were detected. A graphical representation of the dominating families of non-methylotrophic and non-phototrophic bacteria is given in Figure S1. We were unable to detect sequences of nitrifiers in photogranules. Ammonium is therefore likely directly assimilated by the growing biomass. Archaea were only detected in traces in the activated sludge sample before enrichment and otherwise absent in the amplicons.

The postulated trophic chain between the different methylotrophs in photogranules is coupled to the oxygen production by phototrophs, notably cyanobacteria. We analyzed in 23S rRNA amplicons the presence and abundance of cyanobacteria and microalgae. As expected, the total abundance of phototroph sequences in the background activated sludge sample was low compared to photogranule amplicons. Only 370 cyanobacterial sequences were found in activated sludge, whereas the mean cyanobacteria count in photogranules was 49900±6700 (±standard deviation). Microalgal sequences represented the biggest part of the phototrophic population in activated sludge (93%). In photogranules, microalgal sequences were significantly less abundant, accounting for on average 3.5±3.0%. The microalgal population in photogranules was dominated by one single taxonomically unclassified sequence type with a sequence identity over the entire amplicon of approximately 95% to various microalgae genera. This sequence type made up on average 83±26% (median 96%) of the microalgae we found in photogranules. In the activated sludge sample, this particular sequence type was virtually absent (1.2%) in a more diverse microalgal population. It appears that this microalga may be a member specific to the photogranule community, albeit low in abundance compared to cyanobacteria. In the background photogranule and the inocula at the end of the enrichment, three sequence types dominated the cyanobacterial counts were detected, two of which are affiliated with *Leptolyngbya boryana* and one with *Phormidium tenue*. These organisms are filamentous, motile cyanobacteria, as often found to constitute the phototrophic biomass of photogranules (Milferstedt et al., 2017). After the enrichment, 90.0±4.3% of all phototrophic sequences were related to *Leptolyngbya* and 2.9±1.7% to *Phormidium*. During reactor operation, the distribution of the two cyanobacterial types was close to binary in the different photogranules, where either one of the two dominated the photogranule community, as indicated by the high standard deviations around their mean abundances (52±43% *Leptolyngbya* and 46±44% *Phormidium*). A heterogeneous cyanobacterial composition between individual photogranules within the same reactor was observed not unlike our observations for methanotrophic bacteria. When assuming that the two cyanobacteria perform the same ecosystem function, dominance of one over the other may be the result of a random event at the "birth" of the photogranule, e.g., a photogranule developing from a detached *Leptolyngbya*-dominated aggregate that develops into a *Leptolyngbya*-dominated photogranule.

Likewise, it may be possible that the dominance of either *Leptolyngbya* or *Phormidium* results from preferential interactions with other microbes, for example methanotrophs. Curiously, the samples that contain the lowest numbers of methanotrophs (marked with asterisk in Fig. 6a) coincide with the photogranules in which the phototrophic community is dominated by *Leptolyngbya*-like sequences. Potential preferential pairing between microorganisms, as considered in this study within the methylotrophs, may need to be considered at larger phylogenetic scales than uniquely between methylotrophs. The differences between microbial communities of individual photogranules from the same environment emphasize the need to study these systems at the scale of individual photogranules, for example when formulating the conversion process in a mathematical model.

Conclusions

- A methanotrophic-cyanobacterial syntrophy was established in the chassis of existing oxygenic photogranules. This syntrophy was maintained and propagated in a continuously operated reactor, proven by biomass growth and the removal of dissolved methane. We thus demonstrated the feasibility to ecologically engineer a novel photogranule community as potential biocatalyst for dissolved methane removal from anaerobic effluents.
- Photogranule morphology could be controlled in part by adapting hydrodynamic shear in the system, demonstrating that morphology not only depended on the developmental state of the photogranules.
- The established open community not only contained methanotrophic bacteria and phototrophs, but also non-methanotrophic methylotrophs, likely responsible for methanol conversion. Possibly, methanotrophs only incompletely oxidized methane to methanol, enabling the development of a methanol-degrading community, equally fueled by phototrophically generated oxygen.
- Community composition may differ considerably between photogranules, hinting towards cross-feeding between individuals of the photogranule population. This variability needs to be considered in experimental and modeling studies.
- The presence of non-methanotrophic methylotrophs is not problematic if the biotechnological aim was the removal of dissolved methane as post-treatment of anaerobic effluent. If simultaneous molecule recovery was the intention, e.g., methanol production, more specific ways for controlling the activity of the open microbial community would be needed.
- Further research will focus on the treatment of real anaerobic wastewaters effluent in a long-term continuous mode. Nutrient recovery and an increased loading rate need to be studied as a function of temperature. Photogranules may be suitable to remove methane after psychrophilic anaerobic wastewater treatment with increased methane solubility and decreased biological kinetics.

Author Contributions

A.S.S., J.H., R.K., and K.M. designed the conceptualization and experimental methodology. A.S.S. conducted the experiments. A.S.S. and K.M. analyzed the data. A.S.S. and K.M. wrote the manuscript and all authors contributed reviews and revisions.

Declaration of Competing Interest

The authors declare that they have no known competing financial interests or personal relationships

Acknowledgement

The authors gratefully acknowledge the Norwegian Ministry of Education and Research through the university grant program (Norwegian Department of Education) and by the Foundation *Stiftelsen Signe-Marie* (https://www.stiftelsensignemarie.no/), for their support of this research project. We are also grateful to Philippe Sousbie for assisting in reactor development and Anaïs Bonnafous for assisting in DNA extraction during this research. This work was funded by National French Funding Agency ANR project PSST ANR-16-CE04-0001 and Campus France Partenariat Hubert Curien (PHC) Aurora 43048XE.

References

Abouhend, A.S., McNair, A., Kuo-Dahab, W.C., Watt, C., Butler, C.S., Milferstedt, K., Hamelin, J., Seo, J., Gikonyo, G.J., El-Moselhy, K.M., Park, C., 2018. The oxygenic photogranule process for aeration-free wastewater treatment. Environmental Science & Technology 52 (6), 3503–3511. https://doi.org/10.1021/acs.est.8b00403.

Abouhend, A.S., Milferstedt, K., Hamelin, J., Ansari, A.A., Butler, C., Carbajal-González, B.I., Park, C., 2020. Growth progression of oxygenic photogranules and its impact on bioactivity for aeration-free wastewater treatment. Environmental Science & Technology 54 (1), 486–496. https://doi.org/10.1021/acs.est.9b04745.

Arcangeli, J.-P., Arvin, E., 1999. Modelling the growth of a methanotrophic biofilm: Estimation of parameters and variability. Biodegradation 10 (3), 177–191. https://doi.org/10.1023/A:1008317906069.

Bahr, M., Stams, A.J.M., De la Rosa, F., García-Encina, P.A., Muñoz, R, 2011. Assessing the influence of the carbon oxidation-reduction state on organic pollutant biodegradation in algal–bacterial photobioreactors. Applied Microbiology and Biotechnology 90 (4), 1527–1536. https://doi.org/10.1007/s00253-011-3204-8.

Bandara, W.M.K.R.T.W., Satoh, H., Sasakawa, M., Nakahara, Y., Takahashi, M., Okabe, S, 2011. Removal of residual dissolved methane gas in an upflow anaerobic sludge blanket reactor treating low-strength wastewater at low temperature with degassing membrane. Water Research 45 (11), 3533–3540. https://doi.org/10.1016/j.watres.2011.04.030.

Beck, D.A.C., Kalyuzhnaya, M.G., Malfatti, S., Tringe, S.G., Glavina Del Rio, T., Ivanova, N., Lidstrom, M.E., Chistoserdova, L, 2013. A metagenomic insight into freshwater methane-utilizing communities and evidence for cooperation between the Methylococcaceae and the Methylophilaceae. PeerJ 1. https://doi.org/10.7717/peerj.23 e23–e23PubMed.

Beun, J.J., van Loosdrecht, M.C., Heijnen, J.J., 2000. Aerobic granulation. Water Science and Technology 41 (4–5), 41–48. https://doi.org/10.2166/wst.2000.0423.

Biddanda, B., McMillan, A., Long, S., Snider, M., Weinke, A., 2015. Seeking sunlight: Rapid phototactic motility of filamentous mat-forming cyanobacteria optimize photosynthesis and enhance carbon burial in Lake Huron's submerged sinkholes. Frontiers in Microbiology 6, 930. https://doi.org/10.3389/fmicb.2015.00930.

Brandt, E.M.F., Noyola, A., McAdam, E.J, 2019. Control of diffuse emissions in UASB reactors treating sewage. In: de Lemos Chernicharo, C.A., Bressani-Ribeiro, T. (Eds.), Anaerobic Reactors for Sewage Treatment: Design, Construction and Operation. IWA Publishing. https://doi.org/10.2166/9781780409238_0237 (p. 0).

Chistoserdova, L., Kalyuzhnaya, M.G., Lidstrom, M.E., 2009. The expanding world of methylotrophic metabolism. Annual Review of Microbiology 63 (1), 477–499. https://doi.org/10.1146/annurev.micro.091208.073600.

Chon, D.-H., Rome, M., Kim, Y.M., Park, K.Y., Park, C., 2011. Investigation of the sludge reduction mechanism in the anaerobic side-stream reactor process using several control biological wastewater treatment processes. Water Research 45 (18), 6021–6029. https://doi.org/10.1016/j.watres.2011.08.051.

Cookney, J., Mcleod, A., Mathioudakis, V., Ncube, P., Soares, A., Jefferson, B., McAdam, E.J., 2016. Dissolved methane recovery from anaerobic effluents using hollow fibre membrane contactors. Journal of Membrane Science 502, 141–150. https://doi.org/10.1016/j.memsci.2015.12.037.

Dedysh, S.N., Knief, C., 2018. Diversity and phylogeny of described aerobic methanotrophs. In: Kalyuzhnaya, M.G., Xing, X.-H. (Eds.), Methane biocatalysis: Paving the way to sustainability. Springer International Publishing, pp. 17–42. https://doi.org/10.1007/978-3-319-74866-5_2.

Edgar, R.C., Haas, B.J., Clemente, J.C., Quince, C., Knight, R., 2011. UCHIME improves sensitivity and speed of chimera detection. Bioinformatics 27 (16), 2194–2200. https://doi.org/10.1093/bioinformatics/btr381.

Gao, H., Scherson, Y.D., Wells, G.F., 2014. Towards energy neutral wastewater treatment: Methodology and state of the art. Environmental Science: Processes & Impacts 16 (6), 1223–1246. https://doi.org/10.1039/C4EM00069B.

Hatamoto, M., Yamamoto, H., Kindaichi, T., Ozaki, N., Ohashi, A., 2010. Biological oxidation of dissolved methane in effluents from anaerobic reactors using a down-flow hanging sponge reactor. Water Research 44 (5), 1409–1418. https://doi.org/10.1016/j.watres.2009.11.021.

Henze, M., van Loosdrecht, M.C.M., Ekama, G.A., Brdjanovic, D., 2008. Biological Wastewater Treatment: Principles, Modelling and Design. IWA Publishing. https://doi.org/10.2166/9781780401867.

Hodkinson, B.P., Lutzoni, F., 2009. A microbiotic survey of lichen-associated bacteria reveals a new lineage from the Rhizobiales. Symbiosis 49 (3), 163–180. https://doi.org/10.1007/s13199-009-0049-3.

Kalyuzhnaya, M., Xing, X.-H., 2018. Methane biocatalysis: Paving the way to sustainability. Springer. https://www.springer.com/gp/book/9783319748658.

Knief, C., 2015. Diversity and habitat preferences of cultivated and uncultivated aerobic methanotrophic bacteria evaluated based on pmoA as molecular marker. Frontiers in Microbiology 6, 1346. https://doi.org/10.3389/fmicb.2015.01346.

Leak, D.J., Dalton, H., 1986. Growth yields of methanotrophs. Applied Microbiology and Biotechnology 23 (6), 470–476. https://doi.org/10.1007/BF02346062.

Legland, D., Arganda-Carreras, I., Andrey, P., 2016. MorphoLibJ: integrated library and plugins for mathematical morphology with ImageJ. Bioinformatics (Oxford, England) 32 (22), 3532—3534. https://doi.org/10.1093/bioinformatics/btw413.

Lettinga, G., van Velsen, A.F.M., Hobma, S.W., de Zeeuw, W., Klapwijk, A., 1980. Use of the upflow sludge blanket (USB) reactor concept for biological wastewater treatment, especially for anaerobic treatment. Biotechnology and Bioengineering 22 (4), 699–734. https://doi.org/10.1002/bit.260220402.

Liu, L., Fan, H., Liu, Y., Liu, C., Huang, X., 2017. Development of algae-bacteria granular consortia in photo-sequencing batch reactor. Bioresource Technology 232, 64–71. https://doi.org/10.1016/j.biortech.2017.02.025.

Liu, Y., Xu, H.-L., Yang, S.-F., Tay, J.-H., 2003. Mechanisms and models for anaerobic granulation in upflow anaerobic sludge blanket reactor. Water Research 37 (3), 661–673. https://doi.org/10.1016/S0043-1354(02)00351-2.

Liu, Z., Yin, H., Dang, Z., Liu, Y., 2014. Dissolved methane: A hurdle for anaerobic treatment of municipal wastewater. Environmental Science & Technology 48 (2), 889–890. https://doi.org/10.1021/es405553j.

Lobato, L.C.S., Chernicharo, C.A.L., Souza, C.L, 2012. Estimates of methane loss and energy recovery potential in anaerobic reactors treating domestic wastewater. Water Science and Technology 66 (12), 2745–2753. https://doi.org/10.2166/wst.2012.514.

Matsuura, N., Hatamoto, M., Sumino, H., Syutsubo, K., Yamaguchi, T., Ohashi, A., 2015. Recovery and biological oxidation of dissolved methane in effluent from UASB treatment of municipal sewage using a two-stage closed downflow hanging sponge system. Journal of Environmental Management 151, 200–209. https://doi.org/10.1016/j.jenvman.2014.12.026.

McMurdie, P.J., Holmes, S., 2013. phyloseq: An R package for reproducible interactive analysis and graphics of microbiome census data. PLOS ONE 8 (4), e61217. https://doi.org/10.1371/journal.pone.0061217.

Milferstedt, K., Kuo-Dahab, W.C., Butler, C.S., Hamelin, J., Abouhend, A.S., Stauch-White, K., McNair, A., Watt, C., Carbajal-González, B.I., Dolan, S., Park, C., 2017. The importance of filamentous cyanobacteria in the development of oxygenic photogranules. Scientific Reports 7 (1), 17944. https://doi.org/10.1038/s41598-017-16614-9.

Milucka, J., Kirf, M., Lu, L., Krupke, A., Lam, P., Littmann, S., Kuypers, M.M., Schubert, C.J., 2015. Methane oxidation coupled to oxygenic photosynthesis in anoxic waters. The Isme Journal 9, 1991.

Morgenroth, E., Sherden, T., van Loosdrecht, M.C.M., Heijnen, J.J., Wilderer, P.A., 1997. Aerobic granular sludge in a sequencing batch reactor. Water Research 31 (12), 3191–3194. https://doi.org/10.1016/S0043-1354(97)00216-9.

Oshkin, I.Y., Beck, D.A., Lamb, A.E., Tchesnokova, V., Benuska, G., McTaggart, T.L., Kalyuzhnaya, M.G., Dedysh, S.N., Lidstrom, M.E., Chistoserdova, L., 2015. Methane-fed microbial microcosms show differential community dynamics and pinpoint taxa involved in communal response. The ISME Journal 9 (5), 1119–1129. https://doi.org/10.1038/ismej.2014.203.

Quast, C., Pruesse, E., Yilmaz, P., Gerken, J., Schweer, T., Yarza, P., Peplies, J., Glöckner, F.O., 2013. The SILVA ribosomal RNA gene database project: Improved data processing and web-based tools. Nucleic Acids Research 41 (D1), D590–D596. https://doi.org/10.1093/nar/gks1219.

R Core Team, 2020. R: A language and environment for statistical computing. R Foundation for Statistical Computing, Vienna, Austria. http://www.r-project.org/index.html.

Rasouli, Z., Valverde-Pérez, B., D'Este, M., De Francisci, D., Angelidaki, I., 2018. Nutrient recovery from industrial wastewater as single cell protein by a co-culture of green microalgae and methanotrophs. Biochemical Engineering Journal 134, 129–135. https://doi.org/10.1016/j.bej.2018.03.010.

Rice, E.W., Baird, R.B., Eaton, A.D., Clesceri, L.S., 2013. Standard methods for the examination of water and wastewater, 23rd ed. APHA, AWWA, WEF. *20th edn.*.

Schloss, P.D., Westcott, S.L., Ryabin, T., Hall, J.R., Hartmann, M., Hollister, E.B., Lesniewski, R.A., Oakley, B.B., Parks, D.H., Robinson, C.J., Sahl, J.W., Stres, B., Thallinger, G.G., Van Horn, D.J., Weber, C.F., 2009. Introducing mothur: Open-source, platform-independent, community-supported software for describing and comparing microbial communities. Applied and Environmental Microbiology 75 (23), 7537. https://doi.org/10.1128/AEM.01541-09.

Schneider, C.A., Rasband, W.S., Eliceiri, K.W., 2012. NIH Image to ImageJ: 25 years of image analysis. Nature Methods 9 (7), 671–675. https://doi.org/10.1038/nmeth.2089.

Schneider, J., Campion-Alsumard, T.L., 1999. Construction and destruction of carbonates by marine and freshwater cyanobacteria. European Journal of Phycology 34 (4), 417–426. https://doi.org/10.1080/09670269910001736472.

Seghezzo, L., Zeeman, G., van Lier, J.B., Hamelers, H.V.M., Lettinga, G, 1998. A review: The anaerobic treatment of sewage in UASB and EGSB reactors. Bioresource Technology 65 (3), 175–190. https://doi.org/10.1016/S0960-8524(98)00046-7.

Sherwood, A.R., Presting, G.G., 2007. Universal primers amplify a 23 rDNA plastid marker in eukaryotic algae and cyanobacteria. Journal of Phycology 43 (3), 605–608. https://doi.org/10.1111/j.1529-8817.2007.00341.x.

Souza, C.L., Chernicharo, C.A.L., Aquino, S.F, 2011. Quantification of dissolved methane in UASB reactors treating domestic wastewater under different operating conditions. Water Science and Technology 64 (11), 2259–2264. https://doi.org/10.2166/wst.2011.695.

Takeuchi, M., Ozaki, H., Hiraoka, S., Kamagata, Y., Sakata, S., Yoshioka, H., Iwasaki, W., 2019. Possible cross-feeding pathway of facultative methylotroph *Methyloceanibacter caenitepidi* Gela4 on methanotroph *Methylocaldum marinum* S8. PloS One 14 (3). https://doi.org/10.1371/journal.pone.0213535 e0213535–e0213535PubMed.

Tchobanoglous, G., Burton, F.L., Stensel, H.D., 2003. Metcalf, & Eddy. Wastewater engineering: Treatment and reuse. McGraw-Hill (4th ed. revised by George Tchobanoglous, Franklin L. Burton, H. David Stensel.).

van der Ha, D., Bundervoet, B., Verstraete, W., Boon, N., 2011. A sustainable, carbon neutral methane oxidation by a partnership of methane oxidizing communities and microalgae. Water Res. https://doi.org/10.1016/j.watres.2011.03.005.

van der Ha, D., Nachtergaele, L., Kerckhof, F.-M., Rameiyanti, D., Bossier, P., Verstraete, W., Boon, N., 2012. Conversion of biogas to bioproducts by algae and methane oxidizing bacteria. Environmental Science & Technology 46 (24), 13425–13431. https://doi.org/10.1021/es303929s.

Vandevivere, P., 1999. New and broader applications of anaerobic digestion. Critical Reviews in Environmental Science and Technology 29 (2), 151–173. https://doi.org/10.1080/10643389991259191.

Verstraete, W., Beer, D., Pena, M., Lettinga, G., Lens, P., 1996. Anaerobic bioprocessing of organic wastes. World Journal of Microbiology and Biotechnology 12 (3), 221–238. https://doi.org/10.1007/BF00360919.

Wang, Y., Qian, P.-Y., 2009. Conservative fragments in bacterial 16S rRNA genes and primer design for 16S ribosomal DNA amplicons in metagenomic studies. PLOS ONE 4 (10), e7401. https://doi.org/10.1371/journal.pone.0007401.

Whittenbury, R., Phillips, K.C., Wilkinson, J.F., 1970. Enrichment, isolation and some properties of methane-utilizing bacteria. J. Gen. Microbiol. 61, 205–218. https://doi.org/10.1099/00221287-61-2-205.

Wickham, H., Averick, M., Bryan, J., Chang, W., McGowan, L.D., François, R., Grolemund, G., Hayes, A., Henry, L., Hester, J., Kuhn, M., Pedersen, T.L., Miller, E., Bache, S.M., Müller, K., Ooms, J., Robinson, D., Seidel, D.P., Spinu, V., Takahashi, K., Vaughan, D., Wilke, C., Woo, K., Yutani, H., 2019. Welcome to the Tidyverse. Journal of Open Source Software 4 (43), 1686. https://doi.org/10.21105/joss.01686.

Wu, P.-H., Ng, K.K., Hong, P.-K.A., Yang, P.-Y., Lin, C.-F., 2017. Treatment of low-strength wastewater at mesophilic and psychrophilic conditions using immobilized anaerobic biomass. Chemical Engineering Journal 311, 46–54. https://doi.org/10.1016/j.cej.2016.11.077.

Yu, Z., Beck, D.A.C., Chistoserdova, L, 2017. Natural selection in synthetic communities highlights the roles of *Methylococcaceae* and *Methylophilaceae* and suggests differential roles for alternative methanol dehydrogenases in methane consumption. Frontiers in Microbiology 8, 2392. https://doi.org/10.3389/fmicb.2017.02392.